Steady-State Solutions and Multiclass Calibration of Gipps Microscopic Traffic Flow Model

Vincenzo Punzo and Antonino Tripodi

This study addresses the problem of calibration of the Gipps microscopic traffic flow model. The approach consists of first deriving traffic stream models, in the form of steady-state solutions of car-following models, and then fitting such models to stationary traffic data. To this end, traffic stream models for the Gipps model were first attained, and an explicit formula for the flow at capacity as a function of microscopic parameters is provided. Analysis of the models for different combinations of microscopic parameters explains the widely held belief that the Gipps model is unable to reproduce unstable traffic phenomena. To be suitable for model parameter calibration in simulation practice, single-class models were generalized to a multiclass traffic scenario for which a calibration procedure was developed. Once applied to real motorway traffic data, the multiclass scenario proved its effectiveness in terms of error statistics. Values of calibrated parameters were all significant and consistent with expectations. Moreover, they were consistent with the observed aggregate measures (e.g., flow at capacity). Finally, unlike nonstationary, model-based approaches, the computing time required by the multiclass calibration presented is negligible, allowing calibration of a large number of parameters, that is, calibration of different classes of vehicles.

Since the seminal work of Gipps in 1981 (*1*) the car-following model proposed therein has been one of the most widely studied and applied for the microscopic simulation of traffic. In revised forms it is the basis for the simulation of traffic dynamics in several microsimulation programs (*2–5*).

The attractiveness of the model relies on the intuitive assumption behind the formulation and on the obvious physical meaning of parameters, which suggests using common practice values "without resorting to elaborate calibration procedures" (*1*). This last belief seems to be illusory.

Indeed, traffic dynamics result from a number of complex and partially stochastic human–machine interactions. As a consequence, microscopic traffic flow models as well are necessarily only coarse representations of actual driving behaviors. Therefore, even when they have a clear physical meaning, parameters are substantially tools for fine-tuning (approximated) models, to better reproduce the real world. Then the values of parameters that make the model perform at its best do not necessarily coincide with the values of corresponding variables that can be directly observed in the real world. It has been argued (*6*) that this aspect holds for all models developed following an approach that is halfway between a purely deductive and another purely inductive approach, "whereby one first develops (via physical reasoning and/or adequate idealizations and/or physical analogies) a basic mathematical modeling structure and then one fits this specific structure (its parameters) to real data" (*6*). All traffic flow models seem to be of this type.

This limitation has recently been confirmed by studies attempting to calibrate microscopic traffic flow models against real, detailed traffic data (*7, 8*). Such studies have highlighted the limits of these models on the one hand and the need for model calibration on the other. This need cannot be disregarded since microscopic flow models are the basis of traffic microsimulation software.

Actually, microscopic traffic flow models would require, for proper calibration, detailed vehicle trajectory data for a great number of vehicles. Unfortunately, such data are rarely available [Punzo et al. (*9*) provide a review of available data collection techniques]. Hence the use in calibration of widely available aggregate traffic data, such as counts or speeds at detectors, has been proposed (*10*). This use can be addressed in two ways, each with its own limitations.

The first way involves the direct use of microsimulation software. The software has to be interfaced with an optimization algorithm that, through successive simulations, can find the values of parameters that minimize the distance between observed and simulated data. The main difficulty is that this process becomes computationally infeasible with more than a few parameters, even in small networks [see work by Ciuffo et al. (*11*) for an investigation of the problem and related references]. The absence of suitable automatic tools for calibration in commercial simulation software is the main evidence for this problem.

The second way consists in first deriving traffic stream models corresponding to microscopic traffic flow models and then in fitting such models to stationary traffic data (*12*). The main advantage of this second approach is that it allows one to easily calibrate a large number of parameters as well. The main drawback is that it is suitable only for uninterrupted flows. Using these parameters to simulate interrupted flows is likely to provide nonoptimal results.

For the foregoing reasons, despite the restriction to uninterrupted flows, the second approach is the only one that can be used if a large number of microscopic parameters has to be calibrated, for example, if one wants to calibrate parameters of different types of vehicles in a multiclass simulation (which is a common practice).

Hence the second approach to calibration was developed for the widely used Gipps microscopic traffic flow model. To this end, after a review of the Gipps model, the driving behavior at equilibrium of a pair of drivers is investigated. This investigation leads to the

Department of Transportation Engineering, Università di Napoli Federico II, Via Claudio 21, 80125 Napoli, Italy. Corresponding author: V. Punzo, vinpunzo@unina.it.

Transportation Research Record: Journal of the Transportation Research Board, No. 1999, Transportation Research Board of the National Academies, Washington, D.C., 2007, pp. 104–114.
DOI: 10.3141/1999-12

definition of an equilibrium distance–speed function and the related macroscopic models for single-class stationary traffic flows. Then an extension to a multiclass traffic scenario is proposed, which allows the development of a calibration procedure, really suitable for practical implementations, that has been applied to empirical data.

REVIEW OF GIPPS MODEL

The Gipps model (*1*) uses two different transfer functions for reproducing free-flow and car-following conditions.

In the free-flow regime, speed planned for the following instant (i.e., after a time lag τ) is obtained from an inequality of experimental origin that combines two conditions: (*a*) that the speed never exceed the driver's desired speed and (*b*) that acceleration decrease with increasing speed until it becomes null when the desired speed has been reached.

However, the basic idea behind the proper car-following model is that each driver plans his or her speed for time $(t+\tau)$ such that he or she can safely stop even in the event that the leading vehicle suddenly brakes. Indeed, the model assumes that the leader starts braking at time t at a hypothetical constant deceleration rate $\hat{b}$, and the follower starts braking at time $(t+\tau)$ with his or her maximum desired deceleration rate b. The desired value of the follower's speed for time $(t+\tau)$ can be obtained by ensuring that the position of the follower after vehicle stoppage does not exceed the position of the leader minus a distance greater than the physical length of the leader's vehicle.

The switch between the two driving regimes is not explicitly dealt with, and it is driven by a simple rule: at time $(t+\tau)$ the following vehicle, n, adopts a speed that is the minimum between the values given by the two above-mentioned models:

$$v_n(t+\tau) = \min\left\{v_{a,n}(t+\tau), v_{b,n}(t+\tau)\right\}$$

with

$$\begin{cases} v_{a,n}(t+\tau) = v_n(t) + 2.5a_n\tau\left(1-\dfrac{v_n(t)}{V^{\max}}\right)\sqrt{0.025+\dfrac{v_n(t)}{V^{\max}}} \\ v_{b,n}(t+\tau) = F\left(h_n(t), v_n(t), v_{n-1}(t)\right) \end{cases} \quad (1)$$

and

$$F\left(h_n(t), v_n(t), v_{n-1}(t)\right) = -b_n \cdot \left(\frac{\tau}{2}+\theta\right) + \sqrt{b_n^2 \cdot \left(\frac{\tau}{2}+\theta\right)^2 + b_n \cdot \left[2 \cdot \left(h_n(t) - S_n\right) - \tau \cdot v_n(t) + \frac{v_{n-1}(t)^2}{\hat{b}_{n-1}}\right]}$$

where

$v_{a,n}(t+\tau)$, $v_{b,n}(t+\tau)$ = values of follower's speed at time $(t+\tau)$ in case of, respectively, free-flow and car-following conditions;
$v_n(t)$, $v_{n-1}(t)$ = respectively, follower's and leader's speed at time t;
$x_n(t)$, $x_{n-1}(t)$ = respectively, follower's and leader's position at time t;
$h_n(t) = x_{n-1}(t) - x_n(t)$ = space headway between two vehicles at time t;
a_n = follower's maximum desired acceleration rate;
$V^{\max}$ = follower's desired speed;
τ = "apparent reaction time, a constant for all vehicles" (*1*);
θ = additional "comfort" time lag that allows follower not to brake always at his or her maximum desired rate;
S_n = length of vehicle n plus safety margin;
b_n = "most severe braking that driver of vehicle n (i.e., the follower) wishes to undertake" (*1*); and
$\hat{b}_{n-1}$ = follower's estimate of leader's maximum braking rate.

Throughout the paper all deceleration rates, b, must be intended as absolute values; that is, $b = |b|$.

The most natural way to attain a closed mathematical formulation that could predict vehicle positions and speeds for all times is to supplement Equations 1 with

$$\frac{dx_n(t)}{dt} = v_n(t) \quad (2a)$$

The system of differential difference equations (1 and 2a) is not easy to solve. However, Gipps observes that it can be numerically solved in an effective manner by using an integration step equal to the reaction time τ. Then he supplements Equations 1 with the discretization of Equation 2a by a trapezoidal integration scheme:

$$x_n(t+\tau) = x_n(t) + \frac{\tau}{2}\left(v_n(t) + v_n(t+\tau)\right) \quad (2b)$$

In this way the values of speed and position at time $(t+\tau)$ depend only on values at time t and not at the intermediate times. Considering a proper car-following regime [i.e., $v_n(t+\tau) = v_{b,n}(t+\tau)$], Equations 1 and 2b rewritten in a discrete time form lead to the system of two coupled maps that are easy to cope with:

$$\begin{cases} v_n^{k+1} = F\left(h_n^k, v_n^k, v_{n-1}^k\right) \\ x_n^{k+1} = x_n^k + \dfrac{\tau}{2} \cdot v_n^k + \dfrac{\tau}{2} \cdot F\left(h_n^k, v_n^k, v_{n-1}^k\right) \end{cases} \quad (3)$$

Wilson (*13*) recasts this system that describes the joint evolution of positions and speeds as a system that describes the joint evolution of space headways and speeds:

$$\begin{cases} v_n^{k+1} = F\left(h_n^k, v_n^k, v_{n-1}^k\right) \\ h_n^{k+1} = h_n^k + \dfrac{\tau}{2}\left(v_{n-1}^k - v_n^k\right) + \dfrac{\tau}{2}\left[F\left(h_{n-1}^k, v_{n-1}^k, v_{n-2}^k\right) - F\left(h_n^k, v_n^k, v_{n-1}^k\right)\right] \end{cases} \quad (4)$$

This position allows one to find equilibrium solutions in the form of steady-state solutions of the system of Equations 4 (since in Equations 3 the space is always increasing). In general, a state x_e of a dynamic system is an equilibrium state when the system evolution is confined in x_e (for a constant input). In a car-following system there is equilibrium when the following vehicle observes a stationary space headway from the leader, provided the latter maintains a constant

speed, that is, when there are stationary headways and speeds. Therefore, equilibrium points of the system represented by Equations 4, for a constant input (i.e., for a constant speed, v^*, of vehicle $n-1$), are the steady-state solutions of Equations 4:

$$v_n^{k+1} = v_e \qquad h_n^{k+1} = h_e \qquad \forall k$$

The steady-state solution for the follower's speed is the constant input v^*, since from Equations 4 any speed differential between vehicles at time k implies a change of the headway at time $k+1$. Then

$$v_e = v^*$$

Since v_e and h_e are solutions of Equations 4, the first gives

$$v_e = F(h_e, v_e, v_e)$$

Making terms in the last expression explicit, Wilson (*13*) isolates the square root and squares to obtain

$$\left[v_e + b_n\left(\frac{\tau}{2}+\theta\right)\right]^2 = b_n^2\left(\frac{\tau}{2}+\theta\right)^2 + b_n\left[2(h_e - S) - \tau v_e + \frac{v_e^2}{\hat{b}_{n-1}}\right] \quad (5)$$

from which he derives a monotone increasing speed–distance function for the general case of $b_n \neq \hat{b}_{n-1}$:

$$v_e(h_e) = \text{mid}\left[0, \left(\frac{\tau+\theta}{\frac{1}{b_n} - \frac{1}{\hat{b}_{n-1}}}\right)\cdot\left[-1+\sqrt{1+\frac{2(h_e - S)\left(\frac{1}{b_n} - \frac{1}{\hat{b}_{n-1}}\right)}{(\tau+\theta)^2}}\right], V^{\max}\right] \quad (6a)$$

In the case of $b_n = \hat{b}_{n-1}$ he obtains from Equation 5 the following linear expression:

$$v_e = \text{mid}\left[0, \frac{h_e - S}{\tau+\theta}, V^{\max}\right] \quad (6b)$$

Wilson notes that, for a total time lag of 1 s [the value used by Gipps (*1*) for the model validation, i.e., $\tau = 2/3$ and $\theta = \tau/2$], the linear model from Equation 6b corresponds to a 1-s car-following law.

GIPPS STEADY-STATE BEHAVIOR

In this section, the equilibrium distance–speed function, the dual of Equation 6 found by Wilson, is first derived.

This result allows steady-state solutions to be found for the Gipps car-following model in terms of all the traffic stream characteristics, that is, traffic stream models corresponding to the Gipps microscopic model. These solutions are presented in the subsection on single-class traffic stream models, where an explicit formula for road capacity as a function of microscopic parameters is also reported.

Finally, traffic stream models are generalized to multilane, multiclass stationary traffic flows. It will be shown that this step cannot be disregarded if traffic stream models are to be used for calibrating microscopic model parameters. Currently almost all practical applications of microsimulation models deal with mixed flows.

Equilibrium Distance–Speed Function

From Equation 5, a distance–speed function can be easily obtained as a function, Φ, of the equilibrium speed, v_e, of the vector of parameters, $\boldsymbol{\beta}$:

$$h_e = \Phi(v_e, \boldsymbol{\beta}) \qquad \text{with} \qquad \boldsymbol{\beta} = \left(\tau, \theta, b_n, \hat{b}_{n-1}, S\right)$$

Actually by isolating h_e in Equation 5 and simplifying and rearranging terms, the following is obtained (see also Figure 1*a* and *e*):

$$h_e = h^{\text{Gipps}} = S + v_e(\tau+\theta) + \frac{v_e^2}{2}\left(\frac{1}{b_n} - \frac{1}{\hat{b}_{n-1}}\right) \qquad \forall v_e < V^{\max} \quad (7)$$

This law characterizes the space headway between vehicles at equilibrium, that is, when vehicles proceed at the same stationary speed. It is strict increasing in $[0, V^{\max}[$. Instead, for $v_e = V^{\max}$ it is a multivalued function since, independent of how large the open space between vehicles is, the speed given by Equations 1 is limited by $V^{\max}$ (see Figure 1*a* and *e*). That is, when $v_e = V^{\max}$, all the positive values of the headway are admissible. A useful physical interpretation to Equation 7 can be made: given a speed, at equilibrium, the follower observes a spacing from the rear of the leading vehicle equal to the distance he or she travels during his or her reaction time [i.e., $v_e(\tau+\theta)$] plus the difference in meters between his or her stopping distance and that he or she estimates for the leader (i.e., the last term in Equation 7).

This second aliquot of space is the one that really characterizes the model's behavior. Indeed, when the follower estimates that the leader has the same deceleration rate as his or her own (i.e., $b_n = \hat{b}_{n-1}$) and the last term of Equation 7 disappears, the follower starts braking exactly when the front of his or her vehicle reaches the point where the rear of the leader vehicle was at the moment the latter started braking.

Instead, when the follower supposes that the leader has lower braking capabilities than his or her own (i.e., $b_n > \hat{b}_{n-1}$) and the last term in Equation 7 is negative, Equation 7 states that he or she will start braking in a point downstream of the one where the leader has started braking.

It is no accident that the leader's aggressive behavior, which is perceived as risky, is critical for model stability as well. As anticipated by Gipps (*1*), the relative magnitude of braking rates b_n and $\hat{b}_{n-1}$ is the cornerstone for model stability. Indeed, Wilson (*13*) has shown that the condition $b_n < \hat{b}_{n-1}$ (i.e., the follower's conservative behavior) is a necessary condition for linear stability of the model.

Therefore Equation 7 permits qualitative interpretation of the model stability behavior (and of the boundary definition between stability and instability regions) based on the relative magnitude of braking rates b_n and $\hat{b}_{n-1}$. In the following subsection it will be shown that the relationship between b_n and $\hat{b}_{n-1}$ affects the form of the traffic stream models derived from the Gipps car-following model.

Single-Class Traffic Stream Models

Starting from the functions in Equations 6 and 7 that describe the relationship at equilibrium between distances and speeds of a couple of vehicles, it is straightforward to define stationary models in terms of flow, speed, and density for a single-class traffic flow. To derive traffic stream models from Equations 6 and 7 stated for a couple of vehicles, it will be assumed that all the vehicles have the same parameter values. Moreover, subscripts will be removed. Finally, flow, speed, and density will be expressed, respectively, in vehicles per hour, kilometers per hour, and vehicles per kilometer.

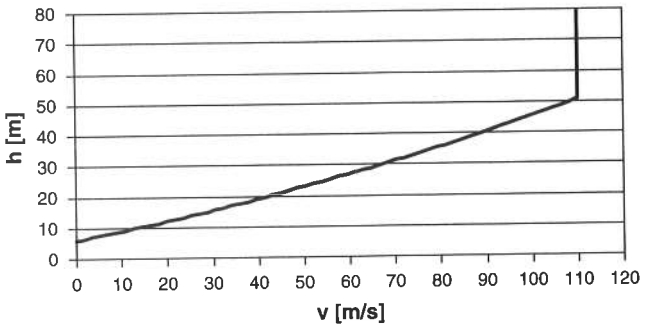

(a)

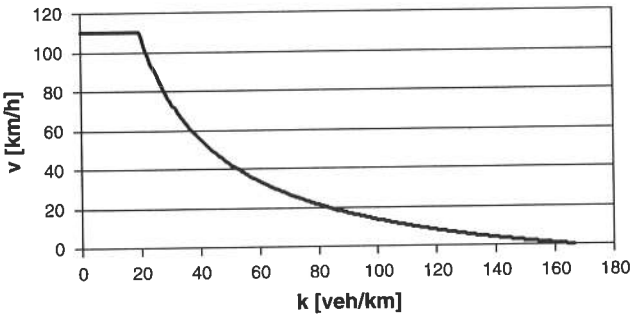

(b)

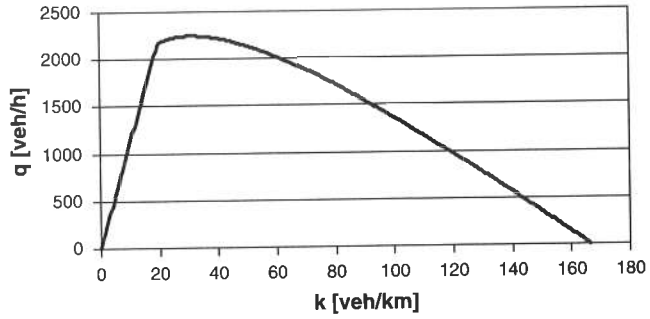

(c)

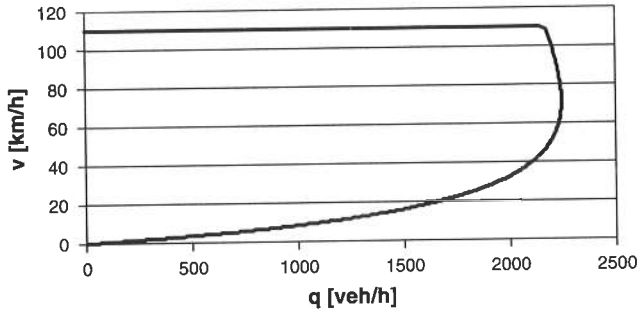

(d)

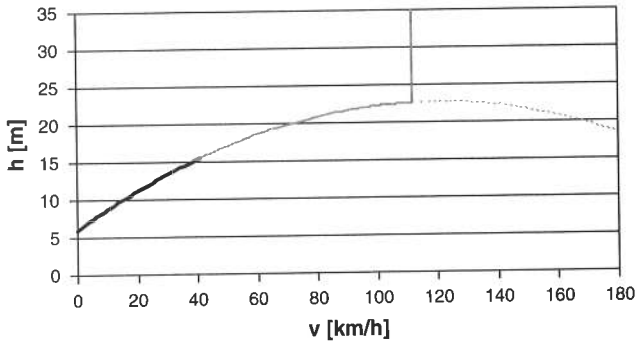

(e)

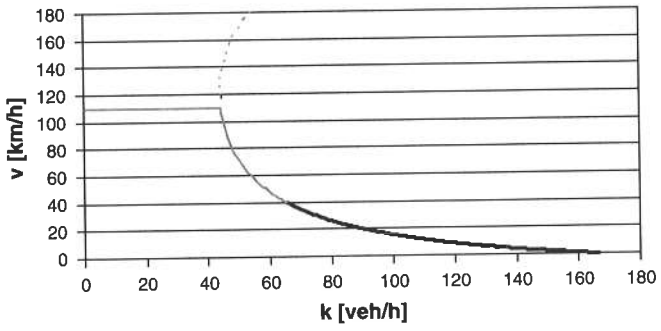

(f)

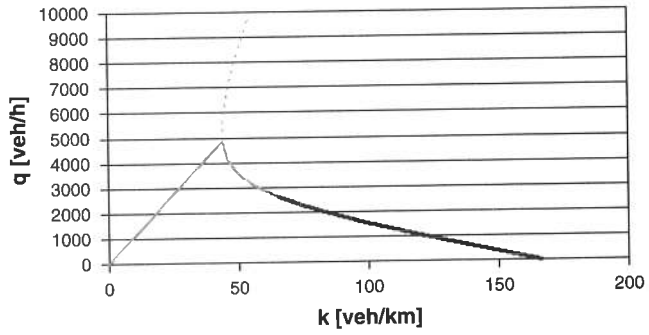

(g)

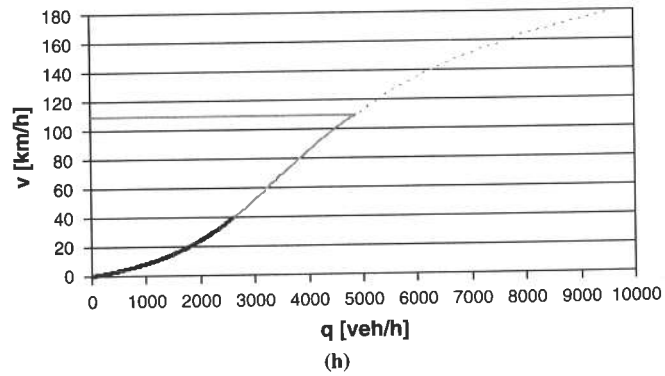

(h)

FIGURE 1 Gipps stationary models: (*a–d*) for $b < \hat{b}$ and (*e–h*) for $b > \hat{b}$.

As previously seen, the speed–distance function assumes different forms for different values of braking rates b and $\hat{b}$: Equation 6a if $b \neq \hat{b}$, and Equation 6b if $b = \hat{b}$. However, even when $b \neq \hat{b}$, depending on $b < \hat{b}$ or $b > \hat{b}$, the shape of both functions 6a and 7 varies, since the term $(1/b - 1/\hat{b})$ changes sign.

For these reasons, traffic stream models will assume different shapes depending on the sign of the term $(1/b - 1/\hat{b})$. Then the most general cases $b < \hat{b}$ and $b > \hat{b}$ will be presented first, followed by the case $b = \hat{b}$.

Case b < b̂

As stated earlier, this case entails conservative behavior on the part of the follower; that is, the follower estimates that the leader has higher braking capabilities than his or her own.

The speed–density model can be easily obtained by Equation 6a:

$$k_e = \frac{1}{\bar{h}} = \frac{1}{h_e} \tag{8}$$

Indeed, the simple substitution of h_e given by Equation 8 in Equation 6a yields (see Figure 1*b*)

$$v_e = \min\left\{3.6\frac{\tau+\theta}{\left(\frac{1}{b}-\frac{1}{\hat{b}}\right)}\left[-1+\sqrt{1+\frac{2\left(\frac{1000}{k_e}-S\right)\left(\frac{1}{b}-\frac{1}{\hat{b}}\right)}{(\tau+\theta)^2}}\right], V^{\max}\right\} \tag{9}$$

Considering the fundamental equation of traffic flow, $q = k\bar{v}_s$ (which strictly holds for stationary traffic), the flow–density relationship is easily obtained by multiplying Equation 9 by the density k_e (see Figure 1*c*). Finally, substitution of Equation 7 in Equation 8 and the ensuing expression for k_e in the fundamental equation results in the flow–speed relationship (see Figure 1*d*):

$$q_e = k_e \cdot v_e = \frac{v_e}{h_e} = \frac{1{,}000 \cdot v_e}{S + \frac{v_e}{3.6}(\tau+\theta) + \frac{1}{2}\left(\frac{v_e}{3.6}\right)^2\left(\frac{1}{b}-\frac{1}{\hat{b}}\right)} \tag{10}$$

Like Equation 7, function 10 is well defined for v_e belonging to $[0, V^{\max}[$. For $v = V^{\max}$ it is a multivalued function. The derivative of Equation 10 with respect to v_e provides the expression for the speed at capacity:

$$v_{CAP} = 3.6\sqrt{\frac{2S}{\frac{1}{b}-\frac{1}{\hat{b}}}} \tag{11}$$

Finally, if one substitutes Equation 11 in Equation 10 and simplifies, the expression for the flow at capacity is obtained:

$$q_{CAP} = \frac{3{,}600}{\tau+\theta+\sqrt{2S\left(\frac{1}{b}-\frac{1}{\hat{b}}\right)}} \tag{12}$$

In Figure 1*b*, *c* and *d* the shapes of the derived models are reported, with values of parameters equal to $\tau = 2/3$ s, $\theta = 0.5\tau$ [i.e., the same delays used by Gipps (*1*)], $b = 2.75$ m/s², $\hat{b} = 3.0$ m/s², $S = 6$ m, and $V^{\max} = 110$ km/h. They produce values of speed and flow at capacity of, respectively, 71.3 km/h and 2,246 veh/h. Since these values are not derived from the fitting of models to empirical data, the proportions of the diagrams can vary appreciably in practice (compare Figure 4).

It can be observed that the speed–density function is first stationary and then decreases more than linearly. The flow–density function first increases linearly with a slope equal to $V^{\max}$ (i.e., $q = k \cdot V^{\max}$) and then follows the trend given by the product of the first term of minimum in Equation 9 per k. Finally the speed–flow curve shows how free-flow speed is maintained for a long time with flow increasing until it sharply decreases near capacity.

Case b > b̂

Case $b > \hat{b}$ entails aggressive behavior on the part of the follower; that is, the follower estimates that the leader has lower braking capabilities than his or her own.

The equations defining the models are the same as those in case $b < \hat{b}$. However, as anticipated, since the term $(1/b - 1/\hat{b})$ changes sign, the shapes of the functions are completely different, as can be seen in Figure 1*e–h*. Parameter values in the graphs are the same as those for the previous case except for $b = 3.0$ m/s² and $\hat{b} = 2.75$ m/s².

The distance–speed function given by Equation 7 is no longer convex and reaches its maximum for

$$V^* = \frac{\tau+\theta}{\frac{1}{\hat{b}}-\frac{1}{b}}$$

[see also the work by Wilson (*13*) with reference to Equations 6].

Then if $V^{\max}$ is chosen higher than V^*, for $v > V^*$, the spacing between vehicles decreases with the speed increase until it becomes null. Obviously this behavior has no correspondence in practice. Moreover, it makes the traffic stream models unphysical. In particular, for $V^{\max} > V^*$, the speed–density and the flow–density relationships become double-valued. Besides, the values of variables in the curves are unrealistic (e.g., a capacity of about 4,870 veh/h).

Another remark concerns the fact that in case $b > \hat{b}$ the behavior of the steady-state flow is not always stable [for a comprehensive discussion on Gipps car-following model stability, see the work by Wilson (*13*)]. In Figure 1 regions of linear stability and instability of the models are represented respectively by heavy black and light grey curves. It can be observed that instability occurs with the lowest densities and stability with high densities. This finding is exactly the opposite of what is observed in the real world.

Since, as has been seen for $b > \hat{b}$, results in terms of aggregate behavior of traffic flows are unrealistic, it can be said in all certainty that the Gipps model should be used only with an assumption of conservative drivers (i.e., $b < \hat{b}$). As a matter of fact, this assumption forces the model behavior to be stable, which explains the widely held belief that the Gipps model is unable to reproduce unstable phenomena like the breakdown of traffic flows.

Case b = b̂

When $b = \hat{b}$, Equation 7 reduces to

$$h_e = S + v_e(\tau+\theta)$$

Following the same steps as previously, the desired relationships can be easily obtained:

$$v_e = \min\left\{V^{max}, 3.6 \cdot \frac{1{,}000/k_e - S}{\tau + \theta}\right\} \quad (13)$$

$$q_e = k_e \cdot \min\left\{V^{max}, 3.6 \cdot \frac{1{,}000/k_e - S}{\tau + \theta}\right\} \quad (14)$$

$$q_e = k_e v_e = \frac{v_e}{h_e} = \frac{1{,}000 \cdot v_e}{S + \frac{1}{3.6} v_e (\tau + \theta)} \quad (15)$$

Plots for the models are shown in Figure 2, in which the values of the parameters are the same as those for the first case except for $b = \hat{b} = 3.0$ m/s^2.

The resulting shapes of the functions are clearly simplified and seem not very realistic. The most unrealistic result seems to be that shown in Figure 2*d*, where the speed at capacity is "always" equal to the free-flow speed, V^{max} (i.e., independently by values of model parameters and by the value of V^{max}).

Multiclass Traffic Stream Models

Traffic stream models derived in the previous section from the Gipps car-following model have an undoubtedly positive outcome: they analytically relate the model's microscopic parameters to traffic stream characteristics (i.e., to flow, speed, and density), whereas otherwise such a relationship is implicit. In other words, it can be reconstructed numerically only after a number of simulations. For example, given a specific set of parameters, one can derive the corresponding value for the capacity of a road by performing a number of simulations with an excessive demand.

Then one can imagine that the relationships derived allow parameters of microscopic traffic flow models to be calibrated without time-consuming optimization procedures involving numerical simulations of the model itself [see, e.g., the work by Ciuffo et al. (*11*)]. Indeed, in this context model calibration is reduced to the fitting of steady-state models to traffic stream data. The main advantage is that calibrated parameters (i.e., parameters of the fitted models) will be consistent with characteristics such as road capacity. This is the basic idea behind the next section, on microscopic parameter calibration.

One key feature of microscopic traffic modeling is the high level of detail of simulated scenarios, including the ability to simulate different types of vehicles. This feature is fundamental, since it is absolutely necessary to perform multiclass simulations (i.e., to consider at least a light vehicle type and a heavy-vehicle type) to correctly reproduce the dynamics of a mixed flow. Therefore, to be suitable for real applications, or to be suitable for calibrating models used by practitioners, previous steady-state relationships must be generalized to multiclass traffic flows.

It is straightforward to derive such models from Equation 7, which describes the space headway between vehicles in stationary conditions. Indeed, assuming that vehicles from different classes observe different headways, a number of Equations 7 ought to be combined into a single model.

Another useful consideration is that, by the definition of equilibrium, all the vehicles that share a lane travel at the same speed despite their class. Then the traffic scenario shown in Figure 3 is obtained, which deals with double-lane, double-class traffic. All the following derivations refer to this scenario, the extension to

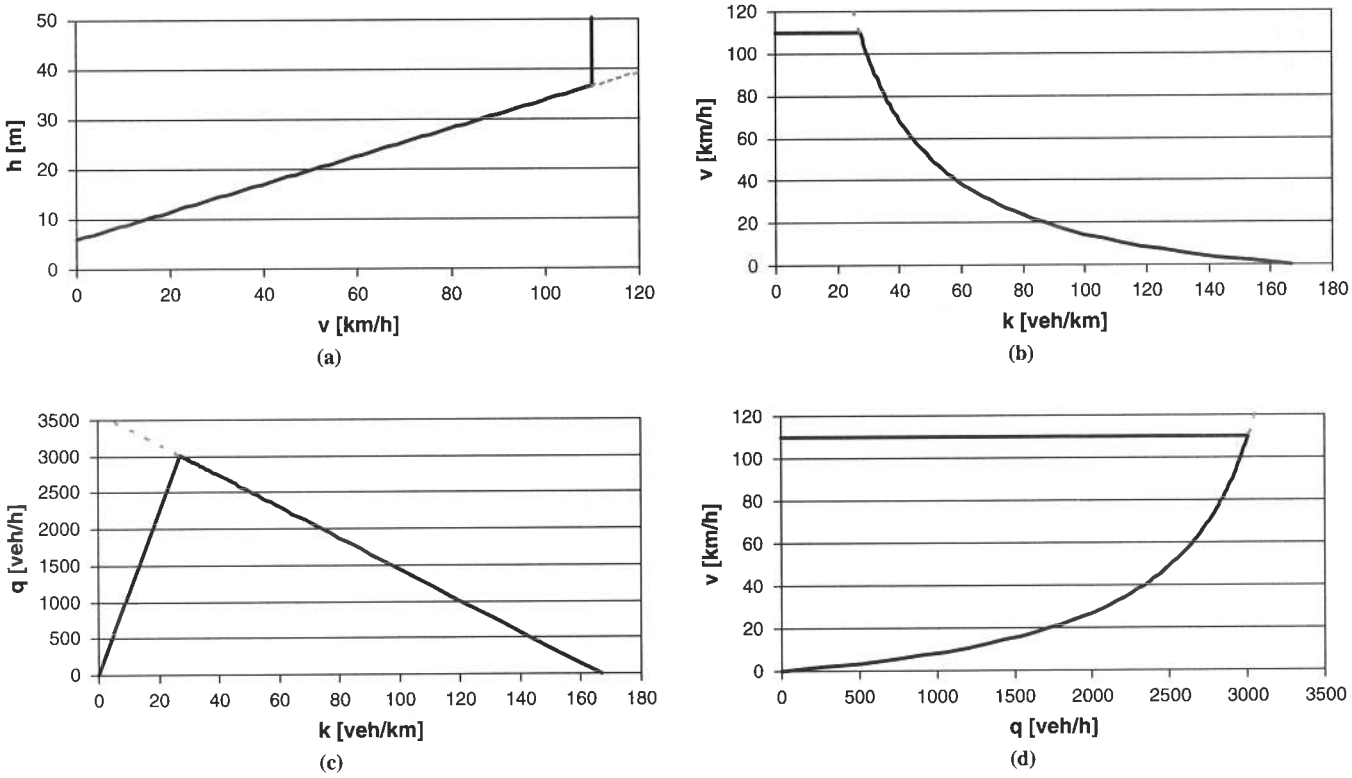

FIGURE 2 Gipps stationary models for $b = \hat{b}$.

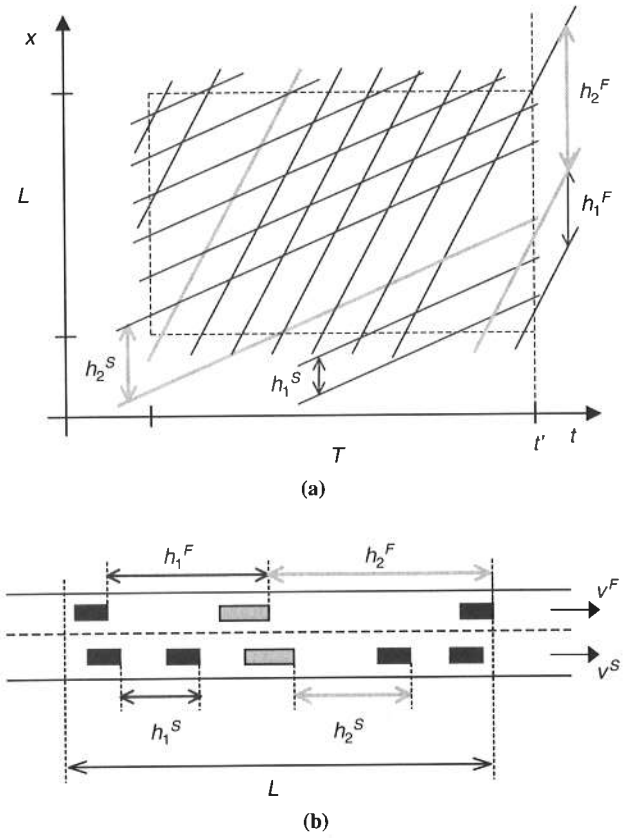

FIGURE 3 Vehicle trajectories for two-lane, two-class stationary traffic scenario: (*a*) in time–space diagram and (*b*) aerial photograph at instant *t'*.

any different combination of number of lanes or vehicle classes being straightforward.

In Figure 3*a* two families of parallel trajectories can be observed, corresponding to the motion of vehicles in two different lanes: a slower lane and a faster lane. Vehicles from different lanes do not interact with one another and proceed at a constant speed shared by all the vehicles of the same lane (as previously stated). Two different classes of vehicles are noted in both lanes: the most numerous class is represented by heavy black straight lines and is called Class 1, and the less numerous one is represented by light gray straight lines and is called Class 2. It is shown that within a lane, vehicles from Class 1 observe on average a smaller space headway than do vehicles from Class 2 (i.e., $h_1 < h_2$). Typically, Class 1 vehicles could represent cars and Class 2, buses or trucks. However, within a class, vehicles in the faster lane observe greater headways than those in the slower lane, having assumed an increasing speed headway function (as in Equation 7).

Figure 3*b* shows an instantaneous picture of the traffic scenario at instant *t'*, like that which would result from an aerial photograph. It is worth noting that, according to Equation 7, vehicles from one class, at a given speed, always observe the same space headway from their leader vehicle regardless of which class their leader vehicle belongs to.

Obviously, with the aim of deriving a stationary model one should agree that the traffic scenario in Figure 3 is stationary. In general, traffic is stationary (in the strict sense) if all vehicle trajectories are parallel and equidistant and also if there is a superposition of families of trajectories with these properties [see work by Daganzo (*14*)]. In such a case, if one inspects the time–space diagram of the traffic along a stretch through a window, the time or location of the window cannot be recognized. This strict definition can be relaxed only by requiring, for stationarity, that the total time spent and the total space traveled by all the vehicles in a window be approximately the same regardless of where the window is placed [for a comprehensive discussion of this position, see work by Daganzo (*14*)]. In the scenario of Figure 3, this less stringent condition of stationarity is verified if one supposes the distribution over space and time of vehicles from different classes to be approximately uniform. Indeed, in such a case, in each window one would have two families of parallel trajectories with approximately the same number of vehicles from the different classes. Therefore it can reasonably be stated that the depicted scenario is stationary.

Nevertheless, this scenario is not far from representing traffic operations on freeways in severely congested conditions (i.e., near capacity). When the flow approximates road capacity, vehicles have difficulty finding a gap in the adjacent lanes to perform a lane change [see work by Brackstone et al. (*15*)]; they proceed at the approximately uniform speed of the lane. Appropriately, this range of operations is the main focus of attention in the calibration here, as will be shown in the next section.

Therefore, given the stationarity of the scenario, it is possible to apply to each lane the fundamental equation:

$$q^l = k^l v^l = \frac{v^l}{\bar{h}^l} \tag{16}$$

where q^l, k^l, v^l, and $\bar{h}^l$ are, respectively, the flow, the density, the speed, and the average space headway on lane l, with $l = S, F$ (i.e., slower and faster lanes).

The average space headway on a lane can be obtained as the average of the headways observed by the vehicles of each class weighted with the percentage of vehicles from that class over the total number of vehicles:

$$\bar{h}^l = \alpha^l h_2^l + (1-\alpha^l) h_1^l$$

where α^l is the percentage of Class 2 vehicles on lane l (i.e., the percentage of heavy vehicles). Since the total density on a lane is equal to the sum of the partial densities (i.e., vehicle densities of each class), $k^l = k_1^l + k_2^l$, α^l can be written as follows (see also Figure 3*b*):

$$\alpha^l = \frac{k_2^l}{k^l}$$

Then Equation 16 becomes

$$q^l = \frac{v^l}{\alpha^l h_2^l + (1-\alpha^l) h_1^l} \tag{17}$$

Substituting Equation 7 in Equation 17—that is, introducing in Equation 17 the expression of the space headway at equilibrium for the Gipps model—one obtains the desired multiclass model:

$$q^{l,\text{Gipps}} = \frac{v^l}{\alpha^l h_2^{l,\text{Gipps}} + (1-\alpha^l) h_1^{l,\text{Gipps}}} \tag{18}$$

where the headway of each vehicle class j, given by Equation 7, is obviously a function of the lane speed, v^l, and of the vector of parameters of that class, $\boldsymbol{\beta}_j$:

$$h_j^{l,\text{Gipps}} = \Phi\left(v^l, \boldsymbol{\beta}_j\right) \quad \text{with} \quad \boldsymbol{\beta}_j = \left(\tau_j, \theta_j, b_{j,n}, \hat{b}_{j,n-1}, S_j\right) \tag{19}$$

From a modeling point of view it is worth noting that parameter values for class j in Equation 19 have to be considered as the mean values for that class. In other words, the proposed model deals with the mean values of the parameter's distributions of each class.

Equation 18 is analogous to Equation 10 for a multiclass traffic flow. Like Equations 7 and 10, it is well defined for v^l belonging to $[0, V^{\max}[$, where $V^{\max} = \min\{V_1^{\max}, V_2^{\max}\}$. For $v^l = V^{\max}$ it is a multivalued function.

MICROSCOPIC PARAMETER CALIBRATION

This section presents a procedure for calibrating the microscopic parameters of the Gipps model based on the multiclass stationary model derived earlier.

Optimal values of parameters are obtained by fitting the multiclass model to real traffic data consisting of detector counts and speeds divided by lane and by vehicle class. The calibration procedure involves the solution of a minimization problem in which the objective function expresses the deviation of the model outputs from the observed measurements. A least-squares (LS) method was implemented.

Methodology

A major difficulty in direct implementation of Equation 18 within an LS estimator is that it is a multivalued function for $v^l = V^{\max}$. This difficulty makes the estimation infeasible. To overcome this problem, the inverse of Equation 18 was considered. However, since Equation 18 is partially invertible, only the part corresponding to stable flows was used, that is, from free-flow conditions to the flow at capacity. This use is consistent with the stationary assumption behind this whole paper.

The resulting expression for lane speed as a function of lane flow, the percentage of heavy vehicles, and the Gipps model parameters for each class is (lane subscript l has been removed for simplicity):

$$v^{\text{Gipps}} = \min\left\{V^{\max}, f\left(q, \alpha, \boldsymbol{\beta}_1, \boldsymbol{\beta}_2\right)\right\} \tag{20}$$

where the second term in the right side is reported in explicit form for the reader's convenience in practical implementation:

$$\begin{aligned} f\left(q, \alpha, \boldsymbol{\beta}_1, \boldsymbol{\beta}_2\right) = {} & \left[90 b_1 \hat{b}_1 b_2 \hat{b}_2 \left[q(1-\alpha)\left(\tau_1 + \theta_1\right) + q\alpha\left(\tau_2 + \theta_2\right)\right.\right. \\ & \left. - 3{,}600\right] - 0.5\left[b_1 \hat{b}_1 b_2 \hat{b}_2 \left[64{,}800 q^2 \left[(1-\alpha)^2 S_1\right.\right.\right. \\ & \left. + \alpha^2 S_2 + \alpha(1-\alpha)\left(S_1 + S_2\right)\right]\left[\alpha b_1 \hat{b}_1 \left(b_2 - \hat{b}_2\right)\right. \\ & \left. + (1-\alpha) b_2 \hat{b}_2 \left(b_1 - \hat{b}_1\right) + 32{,}400 b_1 \hat{b}_1 b_2 \hat{b}_2\right. \\ & \left. \times \left[3{,}600 - q\left[(1-\alpha)\left(\tau_1 + \theta_1\right) + \alpha\left(\tau_2 + \theta_2\right)\right]\right]^2\right]^{0.5}\Big] \\ & \div \left[25q\left[\alpha b_1 \hat{b}_1 \left(b_2 - \hat{b}_2\right) + (1-\alpha) b_2 \hat{b}_2 \left(b_1 - \hat{b}_1\right)\right]\right] \end{aligned} \tag{21}$$

Relationship 20 is plotted in Figure 4*a* and *b* with a continuous heavy black line. In Figure 4 the single-class models given by Equation 10 are reported as well, as continuous light gray lines, the first one fed with the vector of parameters $\boldsymbol{\beta}_1$ and the second one with the vector $\boldsymbol{\beta}_2$, which are the same $\boldsymbol{\beta}_1$ and $\boldsymbol{\beta}_2$ of the mixed-flow model (Equation 20). Figure 4 makes it clear that the model (Equation 20) can be thought of as an interpolation, driven by the percentage of heavy vehicles, α, between the pure model for light vehicles (i.e., if the flow was composed only of light vehicles) and the pure one for heavy vehicles.

On the basis of Equation 20, the LS problem was formulated as follows:

$$\min_{\boldsymbol{\beta}} \gamma = \sum_i \left(v_i^{\text{Gipps}} - v_i^{\text{obs}}\right)^2 \tag{22}$$

where

$\boldsymbol{\beta} = (\boldsymbol{\beta}_1, \boldsymbol{\beta}_2, V_1^{\max}, V_2^{\max})$ = vector of parameters to calibrate,
v_i^{Gipps} = lane speed for interval i obtained by Equation 20,
v_i^{obs} = lane speed observed in interval i,

and index i is retained for the measurement interval.

Since, unlike the current assumption of uniform speed within a lane, observed speeds differ between classes (especially in free-flow conditions), the following position was stated [see work by Daganzo (*14*)]:

$$v^{\text{obs}} = \frac{1}{\dfrac{\delta}{v_2^{\text{obs}}} + \dfrac{(1-\delta)}{v_1^{\text{obs}}}}$$

$$\text{where} \quad \delta = \frac{q_2^{\text{obs}}}{q_{\text{tot}}^{\text{obs}}} \tag{23}$$

Position 23 also defines the relationship between the free-flow speed of the mixed flow, $V^{\max}$, and the free-flow speeds of Class 1 and Class 2 vehicles, $V_1^{\max}$ and $V_2^{\max}$. Otherwise, $V_1^{\max}$ and $V_2^{\max}$ would not take part at all in the optimization problem (Equation 22); that is, it would not be calibrated.

The solving of problem Equation 22 implicitly also provides the breakpoint of the model in Equation 20 between its linear part, $V^{\max}$, and its nonlinear one given by Equation 21. Once optimal parameter values have been found, the breakpoint of Equation 20 divides the flow–speed plane into two parts and then the empirical data into two groups. It is possible to verify that if one knew the groupings before calibration, it would be possible to calibrate separately the two parts of Equation 20, obtaining the same results as with simultaneous calibration. This outcome is relevant since it means that calibration of one branch of the curve (e.g., the one by Equation 21) is not affected by data from the other part of the flow–speed plane, that is, by noncongested data.

In any case, after calibration, it is necessary to verify the assumption behind the LS problem (Equation 22) of homoscedastic data between the groups. Otherwise a generalized LS approach should be adopted.

Application to Empirical Data

The proposed calibration procedure was applied to data collected on the Napoli–Salerno two-lane freeway E45 in Italy. Data consisted of counts and average speeds per class (light and heavy vehicles), per lane per minute. Minute-long measurements were aggregated over longer stationary periods. To this end the constancy of the mean of vehicle

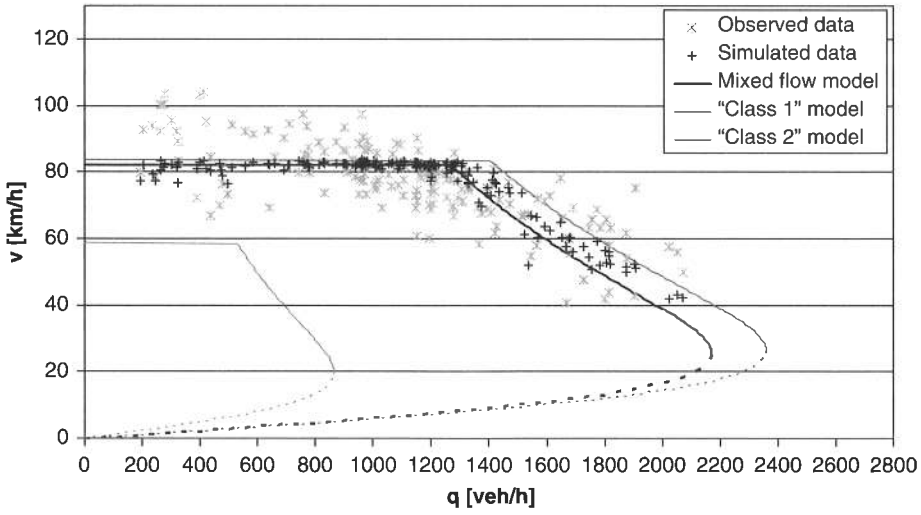

(a)

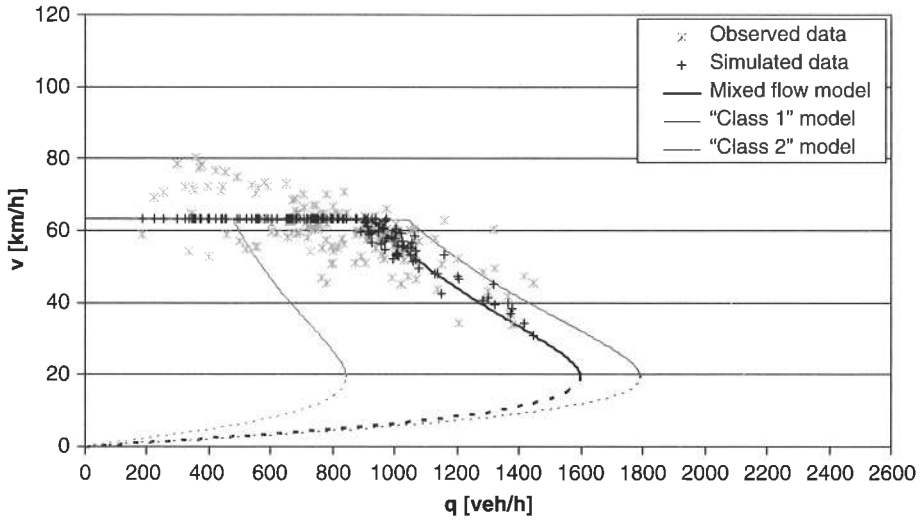

(b)

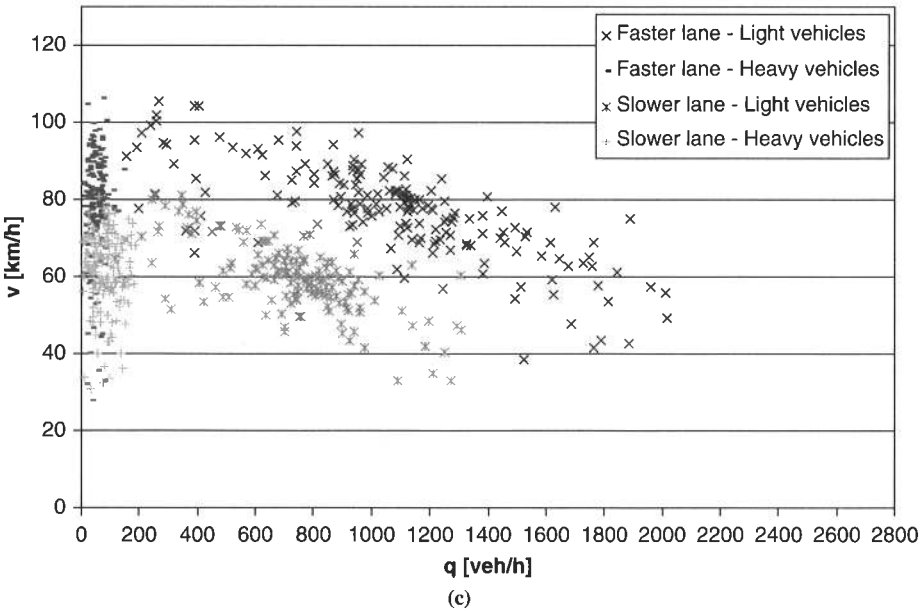

(c)

FIGURE 4 Calibration results on flow–speed plane.

TABLE 1 Calibrated Values of Parameters

Lane	τ_1 (s)	b_1 (m/s²)	$\hat{b}_1$ (m/s²)	V_1^{max} (km/h)	τ_2 (s)	b_2 (m/s²)	$\hat{b}_2$ (m/s²)	V_2^{max} (km/h)
Faster	0.20	1.62	2.35	83.7	0.20	1.12	6.22	58.6
Slower	0.20	1.10	1.77	63.3	0.20	1.00	4.39	63.3

counts, $x_1, x_2, \ldots, x_n$, during successive intervals was checked by using a distribution-free test that verifies the independence of the $x_1, x_2, \ldots, x_n$ sequence from that of the first n natural numbers [see work by Kendall and Stuart (*16*)]. The resulting data are plotted in Figure 4*c*.

A first calibration was performed by assuming that light vehicles (or heavy vehicles) observe the same distance–speed function independent of the lane. This operation entails considering only two classes of vehicles with parameters $\boldsymbol{\beta}_1$, $\boldsymbol{\beta}_2$ and extending the summation in Equation 22 to data from both lanes. The results were not good. For example, a root-mean-square percentage error (RMSPe) of 22.2% was found. But above all, almost all the data were used in fitting only the linear part of the model.

This result suggests that the (manifest) differences existing in this case between data from the two different lanes (see Figure 4*c*) cannot be explained only by the different percentage of heavy vehicles existing on the lanes. That is, light (or heavy) vehicles behave differently if they are in the slower or in the faster lane.

For this reason one model (Equation 20) per lane was successively calibrated. The results are presented in Tables 1 and 2 and in Figure 4*a* and *b*. In the latter, for the faster and slower lanes, observed data (gray stars) are plotted against the values given by Equation 20 after calibration (plus signs). Moreover, in Figure 4*a* (or Figure 4*b*) the mixed-flow model of Equation 20 is plotted for a percentage of heavy vehicles, α, equal to the average of all the observations of the faster (slower) lane. The curve is contained between the pure light and the pure heavy-vehicle curves for that lane.

In Table 1 calibrated values of parameters are reported; in Table 2, error statistics. The latter are root-mean-square error (RMSE), RMSPe, and Theil's inequality coefficients (U, U^M, U^S, U^C) (*17*).

The fitting of all the models is quite satisfactory as confirmed by the error statistics. In particular, Theil's coefficients are near the optimal configuration ($U^M = 0$, $U^S = 0$, $U^C = 1$). This result confirms the belief, from observation of Figure 4*c*, that available data are better reproduced by considering a different model for each lane, that is, four different classes of vehicles: slow cars, slow trucks, fast cars, and fast trucks.

Values of the calibrated parameters seem meaningful and all are consistent with expectations. In particular, the $b/\hat{b}$ ratios that give information on driver aggressiveness were investigated: the lower the ratio, the more conservative the driver is. It can then be verified that trucks are appreciably more conservative than cars, regardless of the lane; that is, trucks observe higher headways. Faster cars (cars in the faster lane) are more aggressive than slower cars. The opposite holds for heavy vehicles that observe slightly greater headways on the fast lane.

Aggressiveness is also affected by reaction time. However, after calibration, all the classes show a reaction time equal to that set as the minimum acceptable value [$\tau = 0.2$ s, having assumed that the θ's were equal to $\tau/2$, as in the work by Gipps (*1*)]. As a matter of fact, smaller reaction times imply that drivers are more aggressive and that the flow at capacity is higher (see Equation 12). One can imagine that calibration produced small reaction times to fit data presenting high values of capacity ("high" must be intended to mean within the limits of the Gipps model in reproducing high capacities).

Finally, the group of data on which the branch of the curve for Equation 21 is fitted is composed mainly of data from heavy congestion, which are presumably scarcely affected by lane changes (*15*). As a result, Gipps microscopic parameters, $\boldsymbol{\beta}$, should not be substantially affected by the fact that lane changing was not considered in the model.

SUMMARY

This study sought to make a contribution to the problem of calibrating the microscopic parameters of the Gipps model. The approach followed consists in first deriving traffic stream models in the form of steady-state solutions of car-following models and then in fitting such models to stationary traffic data.

To this end, the equilibrium distance–speed function for the Gipps car-following model was obtained, and it permitted a qualitative interpretation of the model stability behavior as well. Then corresponding traffic stream models were derived and their analysis, for different combinations of microscopic parameters, allowed the explanation of the widely held belief that the Gipps model is unable to reproduce unstable phenomena like the breakdown of traffic flows (though, from a mathematical point of view, the model can be unstable). An explicit formula for the flow at capacity, as a function of microscopic parameters, was provided as well.

Since multiclass simulations are customary in common practice, single-class models were successively generalized to a multiclass traffic scenario. On the basis of such a mixed-flow model, a calibration procedure was developed and applied to real motorway traffic data. The procedure proved to be effective in terms of error statistics.

TABLE 2 Error Statistics

Lane	RMSE (km/h)	RMSPe (%)	U	U^M	U^S	U^C
Faster	8.97	12.8	0.058	0.000	0.034	0.966
Slower	7.06	12.5	0.059	0.000	0.058	0.942

Values of calibrated parameters were all significant and consistent with expectations. Moreover, they were consistent with the observed aggregate measures (e.g., flow at capacity).

Finally, unlike nonstationary, model-based approaches, the computing time required by the multiclass calibration presented is negligible, allowing calibration of a large number of parameters (i.e., calibration of different classes of vehicles).

ACKNOWLEDGMENT

Traffic data were available under Project 12897 Legge 593/2000 Art.12 PON 2000–2006; TEMA 15–Trasporti: "Sistema di Monitoraggio, Controllo ed Informazione per la Gestione Attiva Della Sicurezza di un'infrastruttura Autostradale."

REFERENCES

1. Gipps, P. G. A Behavioural Car-Following Model for Computer Simulation. *Transportation Research,* Vol. 15B, No. 2, 1981, pp. 105–111.
2. *AIMSUN 5.0 Microsimulator User's Manual 5.0.6.* Transport Simulation Systems, 2005.
3. *SISTM: A Motorway Simulation Model.* Leaflet LF2061. TRL Limited, United Kingdom, 1993.
4. Paramics Microsimulation. SIAS Limited. www.sias.com/sias/home page.html.
5. Wang, J., R. Liu, and F. Montgomery. Car-Following Model for Motorway Traffic. In *Transportation Research Record: Journal of the Transportation Research Board, No. 1934,* Transportation Research Board of the National Academies, Washington, D.C., 2005, pp. 33–42.
6. Papageorgiou, M. Some Remarks on Macroscopic Traffic Flow Modelling. *Transportation Research,* Vol. 32A, No. 5, Sept. 1998, pp. 323–329.
7. Brockfeld, E., R. D. Kühne, A. Skabardonis, and P. Wagner. Toward Benchmarking of Microscopic Traffic Flow Models. In *Transportation Research Record: Journal of the Transportation Research Board, No. 1852,* Transportation Research Board of the National Academies, Washington, D.C., 2003, pp. 124–129.
8. Punzo, V., and F. Simonelli. Analysis and Comparison of Microscopic Traffic Flow Models with Real Traffic Microscopic Data. In *Transportation Research Record: Journal of the Transportation Research Board, No. 1934,* Transportation Research Board of the National Academies, Washington, D.C., 2005, pp. 53–63.
9. Punzo, V., D. J. Formisano, and V. Torrieri. Nonstationary Kalman Filter for Estimation of Accurate and Consistent Car-Following Data. In *Transportation Research Record: Journal of the Transportation Research Board, No. 1934,* Transportation Research Board of the National Academies, Washington, D.C., 2005, pp. 3–12.
10. Toledo, T., M. E. Ben-Akiva, D. Dardar, M. Jha, and H. N. Koutsopoulos. Calibration of Microscopic Traffic Simulation Models with Aggregate Data. In *Transportation Research Record: Journal of the Transportation Research Board, No. 1876,* Transportation Research Board of the National Academies, Washington, D.C., 2004, pp. 10–19.
11. Ciuffo, B., V. Punzo, and V. Torrieri. Framework for Calibrating Microscopic Traffic Simulation Models. Presented at 86th Annual Meeting of the Transportation Research Board, Washington D.C., 2007.
12. Rakha, H., and B. Crowther. Comparison and Calibration of FRESIM and INTEGRATION Steady-State Car-Following Behaviour. *Transportation Research,* Vol. 37A, No. 1, 2003, pp. 1–27.
13. Wilson, E. R. An Analysis of Gipps Car-Following Model of Highway Traffic. *Journal of Applied Mathematics,* Vol. 66, 2001, pp. 509–537.
14. Daganzo, C. F. *Fundamentals of Transportation and Traffic Operations.* Pergamon Press–Elsevier Science, 1997.
15. Brackstone, M., M. McDonald, and J. Wu. Lane Changing on the Motorway: Factors Affecting Its Occurrence, and Their Implications. In *9th International Conference on Road Transport Information and Control,* Conference Publication 454, IEEE, April 1998, pp. 21–23.
16. Kendall, M., and A. Stuart. *The Advanced Theory of Statistics, Vol. 2: Inference and Relationship.* Charles Griffin & Company Limited, London & High Wycombe, 1979.
17. Pindyck, R. S., and D. L. Rubinfeld. *Econometric Models and Economic Forecasts,* 4th ed. McGraw-Hill, New York, 1998.

The Traffic Flow Theory and Characteristics Committee sponsored publication of this paper.